Articles

Synthesis and Characterization of Chromium Silicalite

José Sílvio T. Mambrim,† Heloise O. Pastore,*,† Celso U. Davanzo,† Eduardo J. S. Vichi,*,† Ossamu Nakamura,‡,§ and Helion Vargas‡

Instituto de Química, Universidade Estadual de Campinas, C.P. 6154, Barão Geraldo, 13081-970 Campinas S.P., Brazil, and Instituto de Física Gleb Wataghin, Universidade Estadual de Campinas, C.P. 6165, Barão Geraldo, 13081-970 Campinas S.P., Brazil

Received February 20, 1992. Revised Manuscript Received October 12, 1992

Infrared spectroscopy (mid-IR), ^{29}Si and ^{27}Al magic angle spinning nuclear magnetic resonance (MAS-NMR), powder X-ray diffraction (PXRD), electron paramagnetic resonance (EPR), and photoacoustic spectroscopy (PAS), in combination, have produced useful information about a series of crystalline MFI-type chromium silicalite, synthesized in a fluoride medium. Aluminum is an impurity and occupies framework sites, as evaluated by the ^{27}Al MAS-NMR. The mid-IR spectra are very similar to the zeolite ZSM-5 with the addition of a weak band at $\cong$680 cm^{-1}, which we tentatively assign to symmetric stretching of $(Cr-O-Si)_n$ groups. The samples are crystalline materials and have expanded unit cells, as PXRD measurements pointed out. The as-synthesized sample shows a distribution of Cr sites, detected by EPR, comprising structure and channel occlusion sites; the nonstructural sites being extensively oxidized to Cr(VI) species after calcination in the presence of dioxygen. The changes in the photoacoustically measured physical properties, such as nonradiative relaxation time, the thermal diffusivity and optical absorption coefficient of both calcined and noncalcined chromium silicalite samples are also reported.

Introduction

Zeolitic materials (zeolite-based molecular sieves) containing elements other than aluminum or silicon in the conventional lattice have received increasing attention in recent years,[1] owing to the possibilities offered by the presence of a heteroelement in the structure. From the catalytic point of view, incorporation of elements other than aluminum in the structure is important since the metallosilicate might have its properties fine-tuned for the selective production of desired compounds.[2] Among the characteristics that determine the selectivity, the structure and dimensions of the system of pores and channels[3] (shape selectivity), the Bronsted acidity of sites[4] (quimioselectivity), and the generalized effects arising from differences in the electronegativities of the elements in the structure[5] are the most important. It is well-known that the ZSM-5 structure, with three-dimensional pore network is outstandingly effective in converting methanol to high-octane gasoline.[6] The final mixture is rich in paraffins and aromatics but very poor in olefins.[7] Incorporation of metal atoms other than aluminum can improve dramatically the selectivity of the molecular sieve toward convertion of methanol to olefins,[8-11] this selectivity increasing as the Bronsted sites become less acidic.[8] However, the difficulties in determining the amount of metal incorporated, the thermal stability of the metal in the structure and the difficulty in removing the occluded metallic compounds limit the possibilities of application of these materials in an industrial level.

In this paper, the synthesis, in neutral fluoride medium, of chromium silicalites with MFI structure is described. The products were characterized by chemical analysis, powder X-ray diffraction, infrared spectroscopy, and magic angle spinning nuclear magnetic resonance. The distri-

† Instituto de Química.
‡ Instituto de Física Gleb Wataghin.
§ On leave of absence from Instituto de Física, Universidade Federal da Bahia, 40210 Salvador BA, Brasil.

(1) (a) Gabelica, Z.; Guth, J. L. *Angew. Chem., Int. Ed. Engl.* **1989**, *86*, 81. (b) Kofke, T. J. G.; Gork, R. J.; Kokotailo, G. T. *J. Catal.* **1989**, *116*, 252. (c) Chu, C. T. W.; Chang, C. D. *J. Phys. Chem.* **1985**, *89*, 1569. (d) Wilson, S. T.; Lok, B. M.; Messina, C. A.; Cannan, T. R.; Flanigen, E. M. *ACS Symp. Ser.* **1983**, *218*, 79. (e) Meagher, A.; Nair, V.; Szostak, R. *Zeolites* **1988**, *8*, 3.

(2) (a) Kaeding, W. W.; Butter, S. A. *J. Catal.* **1980**, *61*, 158. (b) McIntosh, R. J.; Seddon, D. *Appl. Catal.* **1983**, *6*, 307. (c) Védrine, J. C.; Auroux, A.; Dejaifve, P.; Ducarme, V.; Hoser, H.; Zhou, S. *J. Catal.* **1982**, *73*, 147.

(3) Guth, J. L.; Caullet, P. *J. Chim. Phys.* **1986**, *86*, 155.

(4) Ward, J. W. *ACS Monograph Ser.* **1976**, *171*, 118.

(5) Mortier, W. J.; Schoonheydt, R. A. *Prog. Solid State Chem.* **1985**, *16*, 1.

(6) (a) Chang, C. D.; Lang, W. H.; Smith, R. L. *J. Catal.* **1979**, *56*, 169. (b) Chang, C. D.; Silvestri, A. J. *J. Catal.* **1977**, *47*, 249. (c) Derouane, E. G.; Nagy, J. B.; Dejaifve, P.; van Hooff, J. H. C.; Spekman, B. P.; Védrine, J. C.; Naccache, C. *J. Catal.* **1978**, *53*, 40. (d) Anderson, J. R.; Foger, K.; Mole, R.; Rajadhyaksha, R. A.; Saunders, J. V. *J. Catal.* **1979**, *58*, 114. (e) Bragin, O. V.; Nefedov, B. K.; Vasina, T. V.; Alekseeva, T.; Lutovinova, V. N.; Minachev, K. M. *Izv. Akad. Nauk SSSR, Ser. Khim.* **1979**, *11*, 2639. (f) Dejaifve, P.; Védrine, J. C.; Bolis, V.; Derouane, E. G. *J. Catal.* **1980**, *63*, 331. (g) Chang, C. D.; Chu, C. T. W. *J. Catal.* **1982**, *74*, 203. (h) Chang, C. D.; Lang, W. H.; Silvestri, A. J. U.S. Patent 4,052,479, 1977.

(7) Morgan, C. R.; Warner, J. P.; Yurchak, S. *Ind. Eng. Chem., Prod. Res. Dev.* **1981**, *20*, 185.

(8) Inui, T.; Matsuda, H.; Yamase, O.; Nagata, H.; Fukuda, K.; Ukawa, T.; Miyamoto, A. *J. Catal.* **1986**, *98*, 491.

(9) Ione, K. G.; Vostrikova, L. A.; Petrova, A. V.; Mastikhin, V. M. *Stud. Surf. Sci. Catal.* **1984**, *18*, 151.

(10) Ione, K. G.; Vostrikova, L. A.; Mastikhin, V. M. *J. Mol. Catal.* **1985**, *31*, 355.

(11) Borade, R. B.; Halgeri, A. B.; Rao, T. S. R. P. *Stud. Surf. Sci. Catal.* **1986**, *28*, 851.

0897-4756/93/2805-0166$04.00/0

Table I. Elemental Analysis (wt %) of As-Synthesized (AS) and Ionic Exchanged (IE) Samples

sample[a]	color	SiO_2	Al_2O_3	Cr_2O_3	Fe_2O_3	Na_2O	SiO_2/Cr_2O_3
Cr-100(AS)[b]	white	81.60	1.00	0.90	0.02	2.41	743
Cr-50(AS)	light green	82.40	0.64	1.70	<0.01	2.28	492
Cr-30(AS)	green	81.30	0.93	1.25	0.04	2.19	165
Cr-100(IE)[c]	white	84.5	0.08	0.01	0.04	0.04	20 000
Cr-30(IE)	very light green	82.4	0.19	0.79	<0.01	0.07	264

[a] Cr-100 is a chromium silicalite sample whose SiO_2/Cr_2O_3 ratio in the reactional mixture is 100. The same for Cr-50 and Cr-30. [b] AS = as-synthesized. [c] IE = ion exchanged.

bution and nature of each Cr(III) site in the material, the metal atom redox characteristics as well as its optical, thermal, and magnetic properties were examined using electron paramagnetic resonance and photoacoustic spectroscopy. Preliminary accounts of this work were published previously.[12,13]

Experimental Section

Synthesis. A mixture of sodium silicate (Riedel de-Haen: 63% SiO_2, 18% Na_2O, and 18% water), ammonium fluoride, chromium nitrate 9-hydrate, and water, in that order, was prepared in the ratio 0.1 (9.5372 g):0.05 (1.8519 g):0.002 (0.6283 g):6.0 (108.09 g), for the synthesis of a sample with SiO_2/Cr_2O_3 ratio of 100 in the initial mixture. The pH was adjusted to 6.5–7.0 with 48 vol % HF. After 2 h of stirring, tetrapropylammonium bromide was added in a 40-mL aqueous solution. The suspension was left to age for 24 h, at 348–353 K, under ambient pressure. The hydrothermal treatment was performed at 443–448 K for 15 days. The crystallized chromium silicalite was then filtered, extensively washed with distilled water until neutral pH, and air-dried. The samples were kept in a desiccator over saturated $CaCl_2$ solution before the measurements. For ion exchanges the following procedure was used: 1 g of the metallosilicalite was slurried in 12.5 mL of a 0.1 M HCl aqueous solution. After 24 h, the samples were washed with distilled water until neutral pH and no Cl^- could be detected in the washings. The material was air-dried. Samples were commonly calcined in a open furnace, for 24 h at 693 K, unless otherwise specified.

Elemental Analysis. The silicalites were analyzed for their Si, Al, Cr, Fe, and Na content by atomic absorption after the samples had been dissolved in HF or melt with sodium carbonate. The results obtained by both methods agree within 0.01% error and are presented in Table I.

Scanning Electron Microscopy (SEM). Samples were dispersed over ordinary double-sided tape, glued to the microscope sample holder, and coated with gold. The accelerating voltage was 25 kV, and the image was obtained from secondary electrons. The scanning microscope was a JEOL Model JSM-T300.

Magic Angle Spinning Nuclear Magnetic Resonance (MAS-NMR). These were collected for ^{29}Si and ^{27}Al in a Brucker AC300/P with Kel-F rotors, using TMS and an acidic $[Al(H_2O)_6]^{3+}$ solution as references, respectively. The frequencies were 59.628 (Si) and 78.206 MHz (Al), and 1100 (Si) and 40 000 (Al) scans were accumulated. The spinning rate was typically 4500 Hz.

Powder X-ray Diffraction (PXRD). The chromium silicalites were analyzed with a Shimadzu diffractometer, Model XD3A (30 kV, 20 mA, 2θ 2° min^{-1}) using Cu Kα radiation. The samples are highly crystalline phase-pure ZSM-5 molecular sieves. They present orthorhombic symmetry when as-synthesized and an orthorhombic-to-monoclinic phase transition upon calcination at 693 K. This phase transition is expected for these SiO_2/T_2O_3 ratios,[12] where T is the general nomenclature for atoms in the framework of zeolites or zeolitic metallosilicalites. For the determination of unit cell volumes, the diffractogram was scanned at 2θ 1° min^{-1}. The (012), (031), (022), (−103), (033), (501), (503), (10 0 0), and (400) diffractions were used to calculate the unit cell volumes for monoclinic samples, while (020), (102), (501), (151), (303), (133), (432), (352), (10 0 0), and (0 10 0) were used for orthorhombic ones.

Table II. Optical Densities Ratios for the Bands at 550 and 450 cm^{-1}, for As-Synthesized (AS) and Calcined (C) Samples

	A^{550}/A^{450}		$\nu[(Si-O-Si)_n]$, cm^{-1}		$\nu[(Si-O-Cr)_n]$, cm^{-1}	
sample	AS	C	AS	C	AS	C
Cr-100	0.75	0.81	793	796	690	689
Cr-50	0.79	0.79	788	799	695	691
Cr-30	0.88	0.82	795	795	696	680

Infrared Spectroscopy (MID-IR). Potassium bromide pellets (0.5 wt %) were measured in a Jasco IR 700 spectrophotometer, the ratio of 550 to 450 cm^{-1} optical densities for as-synthesized (AS) and calcined (C) samples are listed in Table II.

Electron Paramagnetic Resonance (EPR). Spectra were obtained using a Varian E-12 spectrometer operating at 9.5 GHz (X-band). The g values of the samples were obtained with reference to a standard mark: diphenylpycrilhydrazine (DPPH), g value 2.0036. The spectra were recorded on samples at the liquid nitrogen (77 K) and at room temperature (300 K).

Photoacoustic Spectroscopy (PAS). The optical absorption measurements were carried out at room temperature in the wavelength range 300–700 nm using an EDT Model OAS-400 photoacoustic spectrometer. The thermal properties, the nonradiative relaxation time and the optical absorption coefficients were measured by using instrumentation and techniques described previously.[14-16]

Computational Fittings. The ESR experimental data are fitted to theoretical expressions using an IBM 3090 computer. The expressions used are composed of the superposition of symmetrical line shapes with powder pattern line shapes. The routines used for the fittings are those of Bevington.[17]

Results and Discussion

Synthesis. Among the several factors involved in the preparation of metallosilicalites, the form in which the trivalent cation is introduced in the synthesis mixture seems to be one of the most critical. In basic medium, where most of the zeolitic aluminosilicates are prepared,[18,19] the incorporation of other metals is made difficult owing to formation of less-soluble hydroxo compounds, as in the

(12) Pastore, H. O.; Stein, E.; Davanzo, C. U.; Vichi, E. J. S.; Nakamura, O.; Baesso, M.; Silva, E. C.; Vargas, H. *J. Chem. Soc., Chem. Commun.* **1990**, 772.

(13) (a) Mambrim, J. S. T.; Vichi, E. J. S.; Pastore, H. O.; Davanzo, C. U.; Vargas, H.; Silva, E. C.; Nakamura, O. *J. Chem. Soc., Chem. Commun.* **1991**, 141. (b) Nakamura, O.; Mambrim, J. S. T.; Pastore, H. O.; Vichi, E. J. S.; Gandra, F. G.; Silva, E. C.; Vargas, H.; Pelz, J. *J. Chem. Soc., Faraday Trans.* **1992**, *88*, 2071.

(14) Iacovacci, M.; Silva, E. C.; Vargas, H.; Pinheiro, E. A.; Galembeck, F.; Miranda, L. C. M. *J. Appl. Phys.* **1989**, *65*, 5150.

(15) Abrita, T.; Cella, N.; Vargas, H. *Chem. Phys. Lett.* **1989**, *161*, 12.

(16) Nakamura, O.; Mansanares, A. M.; Vargas, H.; Pastore, H. O.; Vichi, E. J. S.; Leite, N. F.; Miranda, L. C. M. Paper P IV/21, *Photoacoustic and Photothermal Phenomena, 7th International Topical Meeting*; Doorwerth: The Netherlands, 1991; p 475.

(17) Bevington, P. R. *Data Reduction and Error Analysis for the Physical Sciences*; McGraw Hill: New York, 1969.

(18) Breck, D. W. *Zeolite Molecular Sieves*; Wiley-Interscience: New York, 1974.

(19) Szostak, R. *Molecular Sieves, Principles of Synthesis and Identification*; Van Nostrand: New York, 1989.

case of iron, or those that do not polycondensate easily as in the case of germanium.[20] In fluoride medium, the pH can be lowered, and less supersaturated reaction mixtures are formed compared to in an alkaline medium,[21] leading to less metastable phases which produce more well-formed crystals. The key point is the formation of soluble metal fluoro complexes which are labile enough to provide a more well-controlled nucleation of the zeolite precursors. For different metal incorporation a compromise between pH and F^- concentration has to be reached, to optimize the synthesis, due to differences in the stability–lability of the different fluorocomplexes. In the chromium silicalite synthesis described in this paper, higher ageing times and higher temperatures are required compared to the used for other metallosilicalites.[22] Several pH and F^- concentrations were checked before using those described in the synthetic procedure, which allowed some but not varied incorporation. The selection of the template used to direct the construction of the skeletal structure is another critical point since a variety of phases can be produced depending on the nature of the template. The tetrapropylammonium bromide salt used in the synthesis of the chromium silicalite described here seems to be the more selective template to direct the construction of MFI-type structures.[21]

Chemical Composition and Crystal Morphology. Apart from the presence of chromium in the samples, the results of the elemental analysis displayed in Table I show that Al_2O_3 is incorporated in the chromium silicalite samples as an impurity, probably coming from the Si source. The location of Al(III) ions in the tetrahedral framework sites is indicated by the ^{27}Al MAS-NMR spectra which show a single and characteristic peak at 52.3 ppm.[23] The presence of Si(OAl) groups in high-silica ZSM-5 structures is confirmed by a peak at −112 ppm in the ^{29}Si MAS-NMR spectra.[23] This peak has shoulders in either higher or lower fields depending on the sample measured, resembling the positions where a high-resolution spectrum would show resolved peaks.[23] However, due to the high SiO_2/Al_2O_3 ratio, none of the shoulders at lower field is in the region expected for Si(1Al).[23] The crystals are rather elongated with sizes varying from 15 to 55 μm on the longer dimension by 14-μm width (Figure 1). In Figure 1b it is possible to observe noncrystallized material adhering to the crystal surface and some extent of intergrowth. Treatment with aqueous HCl was not efficient in dissolving this extraneous material. All the samples are homogeneous, i.e., the crystals present the same morphology from one synthesis batch to another and approximately the same dimensions within the same batch.

Structural Characterization. *Unit Cell Expansion.* The co-incorporation of aluminum and chromium in the silicalite framework is expected to cause a unit cell expansion to an extent proportional to the quantity of these T atoms per silicalite unit cell. Assuming that the T–O–T bond angles do not change with the incorporation of T atoms different from Si in the framework[24] the unit

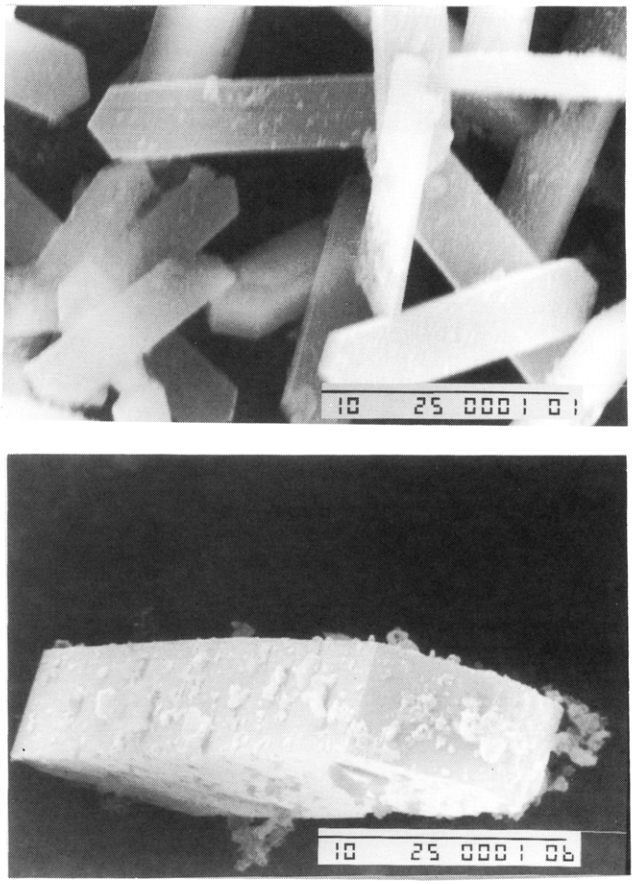

Figure 1. SEM micrographs of (a, top) Cr-30 and (b, bottom) Cr-100.

Table III. Unit Cell Volumes Calculated from XRD for Calcined, V_{xr}(C), and As-Synthesized, V_{xr}(AS), Samples and Calculated from the Aluminum Concentration, V_{calc}

sample	$V_{calc}/10^3$ Å^3	V_{xr}(AS)/10^3 Å^3	V_{xr}(C)/10^3 Å^3
Cr-30	5.31	5.44 ± 0.08	5.43 ± 0.03
Cr-50	5.31	5.51 ± 0.08	5.36 ± 0.03
Cr-100	5.31	5.4 ± 0.1	5.38 ± 0.09

cell expansion can be calculated using eq 1, where V_{Si} is

$$V_x(\mathrm{Al}) = V_{Si} - xV_{Si}[1 - (d_{Al-O}/d_{Si-O})^3] \quad (1)$$

the unit cell volume when T = Si only (5298 Å^3 according to ref 25); V_x(Al) is the unit cell volume of the same lattice where a molar fraction, x, of Si atoms has been replaced by Al atoms; and d_{Al-O} and d_{Si-O} are the related bond distances (1.71[26] and 1.61 Å,[27] respectively). Table III lists the expected unit cell expansion due to Al incorporation only, along with the PXRD-measured cell volume for as-synthesized, V_{xr}(AS), and calcined, V_{xr}(C), chromium silicalites. It is clear that for samples Cr-30 and Cr-50, V_{xr}(AS) is higher, within deviation, than V_x(Al). For sample Cr-100, however, we cannot be sure about chromium(III) incorporation since the expansion might be due solely to aluminum substitution. The same applies to calcined samples: Cr-30 and Cr-50 still have a unit cell volume higher than V_x(Al). The unit cell volume variations are within the range 50–200 Å^3 in excess of the volume

(20) Guth, J. L.; Kessler, H.; Wey, R. *Stud. Surf. Sci. Catal.* **1987**, *33*, 1.
(21) Guth, J. L.; Kessler, H.; Lamblin, J. M.; Patarin, J.; Siene, A.; Chezeau, J. M.; Wey, R. *ACS Symp. Ser.* **1989**, *398*, 176.
(22) For rates of ligand exchange in Cr(III) compounds see: *Mechanisms of Inorganic and Organometallic Reactions*; Twigg, M. V., Ed.; Plenum Press: London, 1990; Vol. 7, p 125, and references therein.
(23) Engelhardt, G.; Michel, D. *High-Resolution Solid State NMR of Silicates and Zeolites*; John Wiley and Sons: New York, 1987.
(24) Bellussi, G.; Millini, R.; Carati, A.; Maddinelli, G.; Gervasini, A. *Zeolites* **1990**, *10*, 642.
(25) Bell, R. G.; Jackson, R. A.; Catlow, R. A. *J. Chem. Soc., Chem. Commun.* **1990**, 782.
(26) Cichocki, A.; Kaczmarska, J. P.; Michalik, M.; Bus, M. *Zeolites* **1990**, *10*, 577.
(27) Cichocki, A.; Datka, J.; Olech, A.; Piwowarska, Z.; Michalik, M. *J. Chem. Soc., Faraday Trans.* **1990**, *86*, 753.

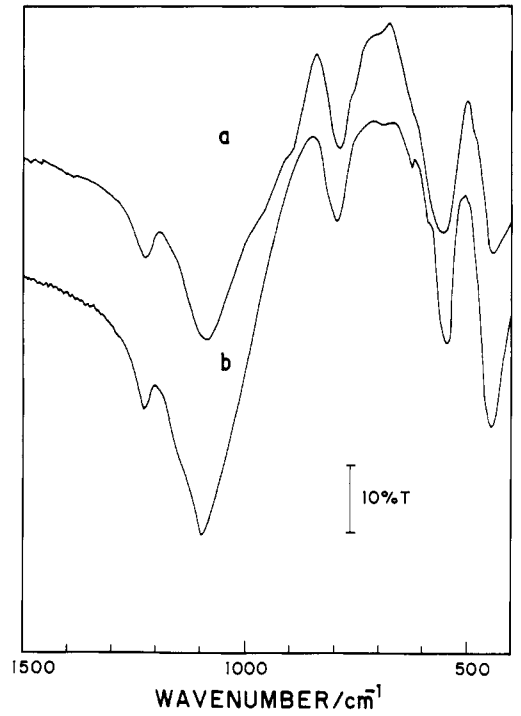

Figure 2. Mid-IR spectra of (a) Cr-100 as-synthesized and (b) Cr-100 calcined for 24 h at 693 K.

calculated taking into account the aluminum incorporation only. This is in agreement with values for the unit cell expansion caused by the incorporation of boron,[28] gallium,[28], aluminum,[28,29] germanium,[30] and titanium[31,32] into the silicalite framework, reported in the literature. Since the length of Cr–O bond in a perfect or distorted tetrahedral symmetry is not yet known, the values for unit cell expansion obtained here for the chromium silicalites cannot be discussed further, except that they provide some evidence for the incorporation of some of the Cr(III) in the silicalite framework.

Crystallinity of the Material and Skeletal Vibrations. IR spectroscopy has been widely used as a technique for the identification of zeolites.[33] Two types of characteristic absorptions are observed in the IR spectra of zeolites; those related to the internal vibrations of the TO_4 tetrahedron, and those related to the vibrations of the skeleton formed by the tridimensional bonding of those tetrahedra. In zeolites with pentasil structure the bands at 450 cm^{-1}, assigned to the internal vibrations of the tetrahedra TO_4 (T = Si, Al) and the band at 550 cm^{-1}, assigned to the vibrations of the secondary building units C_5–T_1 can be used to evaluate the degree of crystallinity of these materials. After Vedrine et al.,[34] a ratio $A^{550}/A^{450} \geq 0.72$ has been widely used as a criterium for high crystallinity of ZSM-5 type zeolites. The A^{550}/A^{450} values obtained for the chromium silicalite prepared in this work are show in Table II and provide further evidence for the high

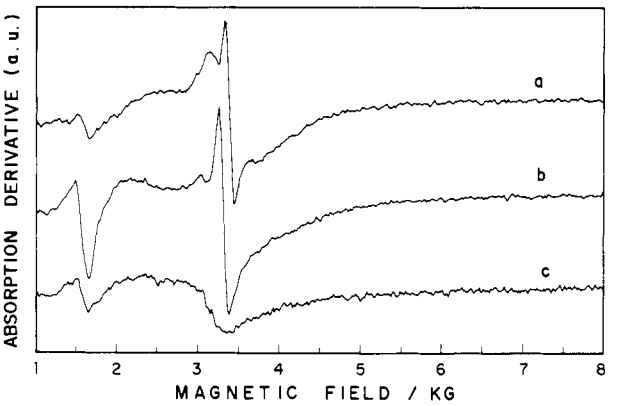

Figure 3. EPR spectra of a silicalite sample (a) as-synthesized at room temperature, (b) as-synthesized at liquid nitrogen temperature, and (c) calcined for 24 h at 693 K.

crystallinity of these materials. The mid-IR spectra of Cr-100 samples, shown in Figure 2, may also provide some evidence for the incorporation of a small amount of Cr(III) in the silicalite framework. The difference in atomic mass of Si(IV) and Cr(III) in the skeleton is enough to pinpoint contributions of (Si–O–Cr) vibrations to the IR spectra. The bands around 795 cm^{-1} in Figure 2 are assigned to the symmetric stretching of the $(Si–O–Si)_n$ group; the very weak bands around 690 cm^{-1} are tentatively assigned to the symmetric stretching of the (Si–O–Cr) group, due to the incorporation of a very small amount of Cr(III) in the framework. These bands are still present in the spectrum after calcination of the material. The frequencies obtained for the samples studied are in Table II. The broadening in the lower wavenumber side of the $(Si–O–Si)_n$ of the as-synthesized sample which could be due to asymmetric vibration of the $(Si–O–Cr)_n$ groups[35] disappear after calcination. Therefore it may be assigned to Si–F and Si–OH, which are expected to show bands in this region.[36] These may condense and be annealed by calcination.[37]

Distribution of the Cr(III) Species in Chromium Silicalite. The EPR study of the materials shows that the Cr(III) ions are distributed in the solid occupying at least three different sites. The assignment of the sites was made by comparing the EPR spectra of pure silicalite and chromium silicalite samples. Figure 3 shows the effect of temperature and calcination on the spectrum of a pure silicalite sample prepared by the same procedure used for the chromium silicalite, without the Cr(III) source. It contains, therefore, nearly the same amount of Fe(III) and Al(III) found in the chromium silicalite. The as-synthesized sample spectra at 300 and 77 K show a broad peak centered at $g \cong 2.0$, superimposed with a sharp signal at $g = 1.97$ (Figures 3a,b). Calcination at 843 K causes a drastic decrease in the intensity of these signals (Figure 3c), suggesting that the signal at $g = 1.97$ is probably due to radicals formed during the synthesis or sample workup. The sharp and weak peak at $g = 4.27$, due to Fe(III) impurities, is not affected by calcination. The spectra of a Cr-30 chromium silicalite sample, at 300 and 77 K, shown in Figure 4, which include resonances at high g values, are interpreted after performing a deconvolution considering the contributions of the symmetrical line centered at $g \cong 2.0$, the background silicalite spectra, and two powder

(28) Rurem, X.; Wenqin, P. *Stud. Surf. Sci. Catal.* **1985**, *24*, 27.
(29) Olson, D. H.; Kokotailo, G. T.; Lawton, S. L.; Meier, W. M. *J. Phys. Chem.* **1981**, *85*, 2238.
(30) Gabelica, Z.; Guth, J. L. *Stud. Surf. Sci. Catal.* **1989**, *49A*, 421.
(31) Chiu, S.; Pang, W.; Yao, S. *Stud. Surf. Sci. Catal.* **1989**, *49A*, 133.
(32) Perego, G.; Bellussi, G.; Corno, C.; Taramosso, M.; Buonomo, F.; Esposito, A. *Stud. Surf. Sci. Catal.* **1986**, *28*, 129.
(33) Flanigen, E. M.; Khatami, H.; Szymanski, H. A. *Molecular Sieves Zeolites I*; Adv. Chem. Ser. 101; Flanigen, E. M., Sand, L. B., Eds.; American Chemical Society: Washington, DC, 1971, p 201.
(34) Coudurier, G.; Naccache, C.; Védrine, J. C. *J. Chem. Soc., Chem. Commun.* **1982**, 1413.
(35) Szostak, R.; Thomas, T. L. *J. Chem. Soc., Chem. Commun.* **1986**, 113; *J. Catal.* **1986**, *101*, 549.
(36) Wood, D. L.; Rabinovitch, E. M. *Appl. Spectrosc.* **1989**, *43*, 263.
(37) Delmotte, L.; Soulard, M.; Guth, F.; Seive, A.; Lopez, A.; Guth, J. L. *Zeolites* **1990**, *10*, 778.

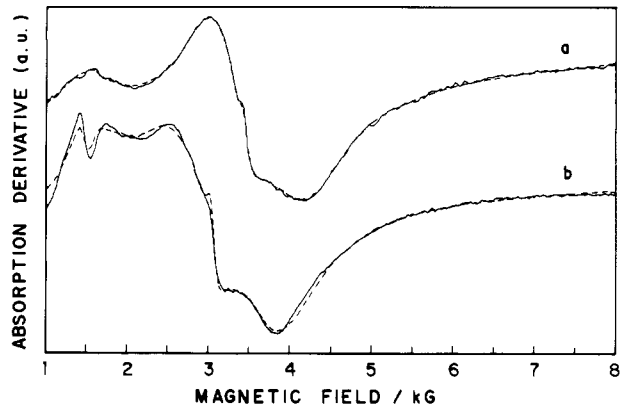

Figure 4. EPR spectra of crystalline zeolitic chromium silicalite, Cr-30 as-synthesized (a) at room temperature and (b) at liquid nitrogen temperature. Dashed lines correspond to the best fit to the experimental curve.

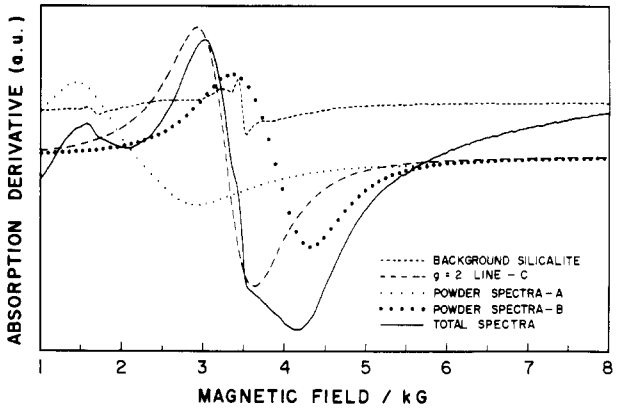

Figure 5. Deconvolution of the experimental EPR curve of crystalline zeolitic chromium silicalite at room temperature. Inset: the main contributions used for the fitting process.

Table IV. g Values for Cr-30, Obtained from the Fitting of the Experimental Spectra

	temp/K		
	300	77	site
g_x[a]	4.49	4.06	
g_y	2.71	2.19	
g_z	1.66	2.03	A
ΔH/kG[b]	0.60	0.43	
A[c]	1.50	1.04	
g_x	2.00	2.61	
g_y	1.67	1.75	
g_z	1.66	1.69	B
ΔH/kG[b]	0.66	0.56	
A[c]	5.23	3.66	
g	2.08	1.88	
ΔH/kG[b]	0.61	1.19	C
A[c]	0.14	0.35	

[a] g value within ±0.3. [b] ΔH is the line width within ±50 G. [c] A is the relative amplitude.

pattern line-shaped spectra, as shown in Figure 5. The dashed lines in Figure 4 correspond to the best fit to the experimental data. For the assignment of the different Cr(III) sites, it was assumed that the powder line shaped resonances are due to two sites, A and B, which suffer the action of crystalline fields with different cubic distortions. The symmetrical line C centered at $g \cong 2.0$ is assigned[38] to the ion-exchange cations $[Cr(H_2O)_6]^{3+}$ and to chromium oxide-like compounds occluded in the channels, outside

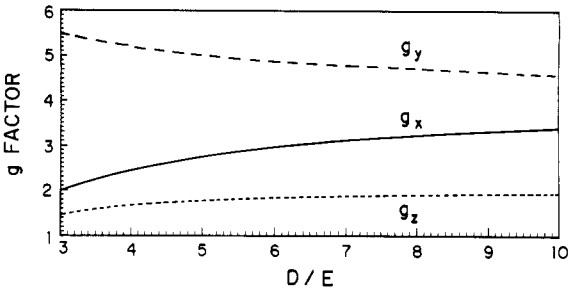

Figure 6. Theoretical prevision of effective g factor in the x, y, and z directions as a function of the ratio D/E.

the silicon framework. The EPR parameters for these different sites, shown in Table IV, are obtained by experimental fitting using the line width and the amplitude as adjustable parameters. The Cr(III) species in site C suffer no constraints and are expected to interact, the interaction between them being usually stronger as temperature decreases. In fact, the line centered at $g \cong 2.0$ shows a severe increase in line width as the temperature drops from 300 to 77 K, clearly indicating smaller spin relaxation times. The line widths of the lines A and B are not significantly affected by changes in measurement temperature, indicating, as expected, a lower interaction between the Cr(III) species located in those sites.

Identification of the Cr(III) Species in Sites A and B. Assuming that the Cr(III) species, having an $L = 0$ value associated to its orbital ground state, are located in cubic crystalline fields tetrahedrally distorted, the positions of the EPR spectrum lines can be calculated by solving the spin Hamiltonian in eq 2, where the parameters D and E

$$\mathcal{H} = g\beta HS + D[S_z^2 - (S/3)(S+1)] + E(S_x^2 - S_y^2) \qquad (2)$$

represent the axial and the rhombic distortions of the octahedron, respectively. The interaction of the Cr^{3+} ions, which have d^3 electron configuration ($L = 3$, $S = {}^3/_2$), with the cubic crystalline field is strong and is the principal term determining the energy levels. Since the spin–orbit interaction and the crystalline field distortions act on the singlet orbital, the Zeeman term will split the two Kramer doublets and the energy levels will depend on the magnetic field and, consequently, on D and E.[39] Several transitions may occur between the levels for each direction of the magnetic field, and Figure 6 shows the expected g value as a function of D/E ratio for a particular direction of the magnetic field. For $D/E = 6.5$ and $f = 9.54$ GHz at room temperature, one finds a set of g values in good agreement with those obtained for site A (see Table IV), confirming that Cr(III) is substituting Si(IV) in the silicalite skeleton. The assumptions made in the previous calculations do not provide any solution for site B, indicating that this is not a skeleton site but probably a highly distorted species trapped inside the channels. To distinguish both situations, the as-synthesized samples were ion-exchanged three times with aqueous 0.01 M HCl, for 24 h at 80 °C. The EPR spectra of the ion-exchanged samples, shown in Figure 7, did not display site B peak anymore, showing that the Cr(III) species was washed away. Moreover the line corresponding to site C diminished considerably, making site A even more distinguishable. In line with this observation the weak band at ca. 680 cm^{-1} in the mid-IR spectrum is still present for the ion-exchanged material,

(38) Pearce, J. R.; Sherwood, D. E.; Hall, M. B.; Lunsford, J. H. *J. Phys. Chem.* **1980**, *84*, 3215.

(39) Fuxi, G.; He, D.; Huiming, L. *J. Non-Cryst. Solids* **1982**, *52*, 135.

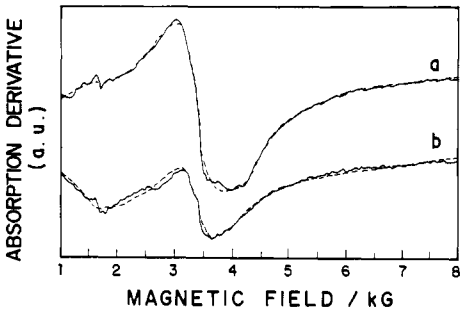

Figure 7. EPR spectra of chromium silicalite Cr-100 (a) as-synthesized, and (b) three times ion-exchanged with HCl solution. The dashed lines correspond to the best fit to the experimental curve.

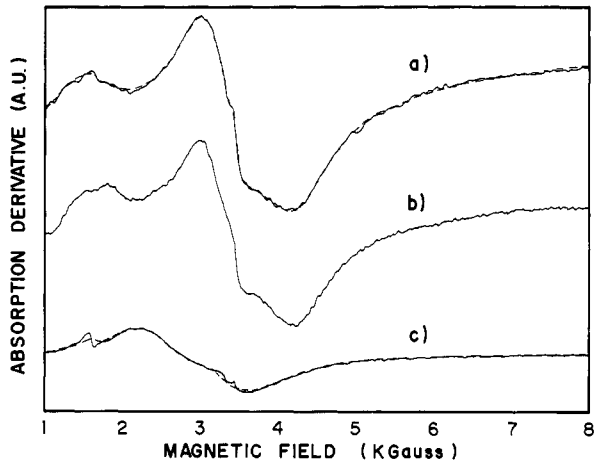

Figure 8. EPR spectra of the chromium silicalite, Cr-30, (a) as-synthesized, (b) calcined at 693 K for 24 h, and (c) calcined for 24 h at 843 K.

supporting our previous assumption that this band is due to $(Si–O–Cr)_n$ group symmetric stretching.

Oxidation of Extraframework Cr(III) to Cr(VI). Calcination of a Cr-30 sample for 24 h, at 693 and 843 K, under oxygen flow, leads to incorporation of oxygen by the sample with oxidation of Cr(III) to Cr(VI) species.[13] A comparison of the EPR spectra of a sample as-synthesized and after calcination at 693 K (Figure 8) shows that they display essentially the same features except by a change in the relative intensities of the peaks within g = 2.08 and 1.66 related to sites C and B, respectively. In spectrum 8b, the relative intensity B/C is higher than for spectrum 8a, showing that Cr(III) species in site C (channels) were oxidized to EPR-silent Cr(VI) species. Calcination at 843 K leads to the complete oxidation of all sites and structure collapse. The effects of calcination in the IR and photoacoustic spectra were also examined. The IR spectra in Figure 9 show that the sample calcined at 693 K retained its MFI structure as determined by the A^{550}/A^{450} optical density ratio equal to 0.77 for 9a and 0.74 for 9b. However, calcination at 843 K leads to the collapse of the crystal structure of the pentasil zeolite, as shown by the disappearance of the peaks at 550 and 450 cm^{-1} in Figure 9c. The photoacoustic spectra of the Cr-30, as-synthesized and calcined at 693 K, are shown in Figure 10. The as-synthesized sample shows two bands centered at 440 and 640 nm, assigned to the $^4A_2 \rightarrow {}^4T_1(F)$ and $^4A_2 \rightarrow {}^4T_2$ transitions, respectively, characteristic of Cr(III) species. After calcination at 693 K a strong band at 370 nm is observed, which is assigned to a charge-transfer absorption of Cr(VI). In Figure 10c it is possible to observe

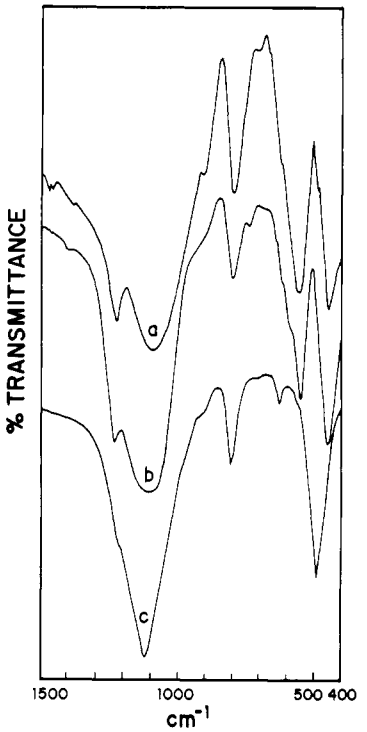

Figure 9. Mid-IR spectra showing the effect of calcination at increasing temperatures upon the zeolitic lattice integrity of sample Cr-30 (a) as-synthesized, (b) calcined for 24 h at 693 K, and (c) calcined for 24 h at 843 K.

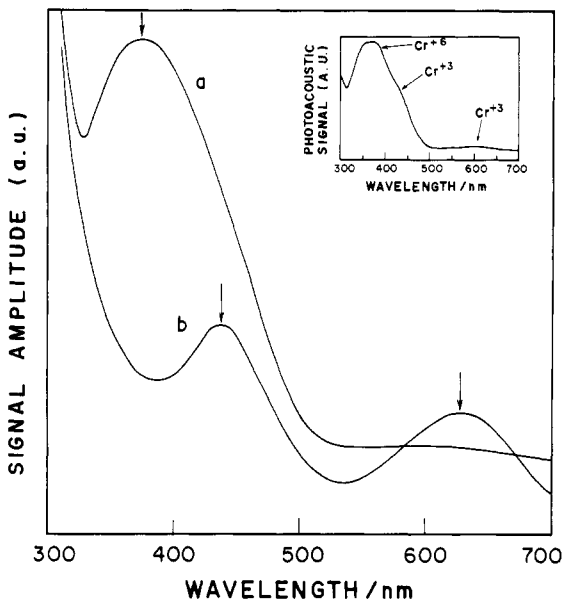

Figure 10. PA spectra of chromium silicalite Cr-30, (a) calcined at 693 K, (b) as-synthesized, and (inset) after extensive calcination at 693 K (on top). Arrows indicate the presence of two absorbing centers.

the very weak Cr(III) bands in the presence of Cr(VI), which provides a strong evidence that even after extensive calcination at 693 K some Cr(III) still remains in the chromium silicalite, very likely the ones in Si(IV) substitutional sites. It is interesting to note that Fe(III) species in the silicalite framework are stable to reduction, while Fe(III)-O species housed in the channels are reduced by H_2 or CO to EPR-silent Fe(III) species.[40] Therefore, redox cycles involving skeletal transition metal ions might not be as easy as one would expect based on solution chemistry.

Thermal Characterization. Apart from providing direct optical spectra, the photoacoustic technique can

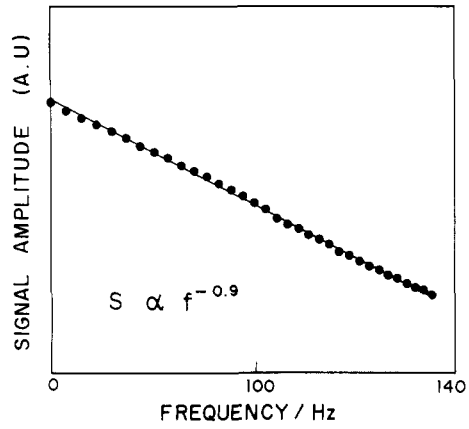

Figure 11. PA rear-signal amplitude for the Cr-30 sample as a function of the modulation frequency, showing the f^{-1} frequency dependence.

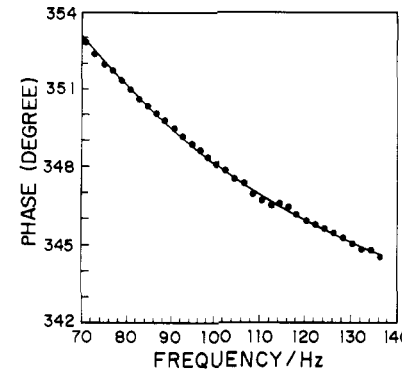

Figure 12. PA rear-signal phase dependence on the modulation frequency for the calcined Cr-30. The solid line corresponds to the data fitting to eq 3.

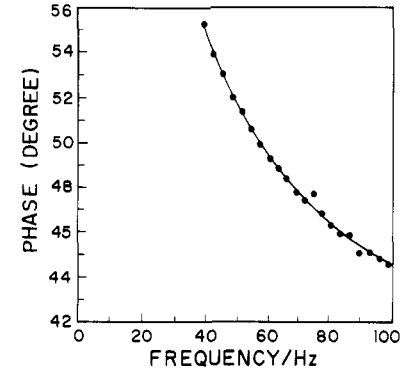

Figure 13. PA phase versus the modulation frequency at the 440-nm wavelength for the as-synthesized Cr-30. The solid line corresponds to the data fitting to eq 4.

also be used in the characterization of thermal properties[41,42] as well as in the investigation of nonradiative relaxation processes.[15,43,44]

Thermal Diffusivity. Like the optical absorption, the thermal diffusivity, α, is unique for each material and has been determined for a wide range of them, such as metals, minerals, and biological specimens.[45] Furthermore, α is extremely dependent upon the effects of compositional and microstructural variables[46] as well as processing conditions as in the case of polymers,[47,48] ceramics,[49] and glasses.[49] The thermal diffusivities of the as-synthesized and calcined chromium silicalites were determined by photoacoustic spectroscopy, PA, using the signal data as a function of modulation frequency, f. By performing a rear-illumination signal amplitude measurement, we have determined that the thermal bending mechanism[42,50] is the main reason for the detected PA signal in the modulation range of our experiments; i.e., the rear signal amplitude varies as f^{-1}. This is the expected modulation frequency dependence of the rear signal for a thermally thick sample when the thermoelastic bending dominates the PA signal. In Figure 11 the PA rear-signal amplitude is plotted versus the modulation frequency for a Cr-30 calcined sample. A similar dependence is observed for the as-synthesized sample. The thermal diffusivity is obtained by fitting the front phase signal data to eq 3,

$$\phi = \phi_0 + \arctan [1/(z-1)] \qquad (3)$$

where $z = a(f)^{1/2}$, with $a = (\pi l^2/\alpha)^{1/2}$, l being the sample thickness. Assuming ϕ_0 and a as adjustable parameters, the thermal diffusivity is obtained from the phase data fitting from the parameter α. In Figure 12 the PA signal phase data for the calcined sample is shown as a function of the modulation frequency. The solid curve represents the fitting of the experimental phase data to the theoretical eq 3. The value of α obtained from the data fitting is 0.041 ± 0.002 cm^2 s^{-1}. The same procedure was used for the as-synthesized sample, giving a value of α of 0.038 ± 0.002 cm^2 s^{-1}.

Nonradiative Relaxation Processes. The PA signal also depends upon the light-into-heat conversion efficiency. This means that the PA signal is sensitive to the nonradiative deexcitation process which takes place after the absorption of the incident radiation. Information on the nonradiative deexcitation processes are obtained from the measurements of the PA phase angle as a function of the modulation frequency. For a thermally thick sample, the modulation frequency dependent part of the phase of the PA signal varies as shown in eq 4,[47] where τ is the

$$\phi = -\pi/2 - \arctan(\omega\tau) - \arctan[(2/\omega\tau_\beta)^{0.5} - 1]^{-1} \qquad (4)$$

nonradiative relaxation time, $\tau_\beta = (\beta^2\alpha)^{-1}$ is the thermal diffusion time within the optical absorption depth β^{-1}, and ω is the modulation frequency. Equation 4 shows that the phase change of the PA signal with the modulation frequency of a given absorption band depends not only on its nonradiative relaxation time but also on the thermal diffusion time within the optical parameter depth. This modulation frequency has been used by several authors for studying the behavior of τ in collisional deactivation of vibrational excitation in gases and radiationless relax-

(40) (a) Ball, W. J.; Dwyer, J.; Garforth, A. A.; Smith, W. J. *Stud. Surf. Sci. Catal.* **1986**, *28*, 137. (b) Kustov, L. M.; Kazansky, V. B.; Ratnasamy, P. *Zeolites* **1987**, *7*, 79. (c) Calis, G.; Frenken, P.; Boer, E.; Snolfs, A.; Hefni, M. A. *Zeolites* **1987**, *7*, 319. (d) Meagher, A.; Nair, V.; Szostak, R. *Zeolites* **1988**, *8*, 3.
(41) Adams, M. J.; Knikbright, G. F. *Analyst* **1977**, *102*, 678.
(42) Leite, N. F.; Cella, N.; Vargas, H.; Miranda, L. C. M. *J. Appl. Phys.* **1987**, *61*, 3023.
(43) Quimby, R. S.; Yen, W. M. *J. Appl. Phys.* **1980**, *51*, 1780.
(44) Pessoa, O., Jr.; Cesar, C. L.; Patel, N. A.; Vargas, H.; Chizoni, C. C.; Miranda, L. C. M. *J. Appl. Phys.* **1986**, *59*, 1316.
(45) Touloukian, Y. S.; Powell, R. W.; Ho, C. Y.; Nicolau, M. C. *Thermal Properties of Matter*; Plenum: New York, 1973; Vol. 10.
(46) Merté, B.; Korpium, P.; Lüsher, E.; Tilgner, R. *J. Phys. (Paris) Colloq.* **1983**, *6*, C463.
(47) Torres Filho, A.; Leite, N. F.; Miranda, L. C. M.; Cella, N.; Vargas, H. *J. Appl. Phys.* **1989**, *66*, 97.
(48) Ziegler, G.; Hansselman, A. P. H. *J. Mater. Sci.* **1981**, *16*, 495.
(49) Bento, A. C.; Vargas, H.; Aguiar, M. M. F.; Miranda, L. C. M. *Phys. Chem. Glasses* **1987**, *28*, 127.
(50) Rousset, G.; Lepoutre, F.; Bertrand, L. *J. Appl. Phys.* **1983**, *54*, 2383.

Table V. Values of the Nonradiative Relaxation Time, τ, the Characteristic Diffusion Time, τ_β, and the Optical Absorption Coefficient, β, for the Calcined and As-Synthesized Chromium Silicalite Cr-30

	as-synthesized		calcined
λ (nm)	440	640	380
τ (ms)	2.70 ± 0.35	2.17 ± 0.12	2.26 ± 0.09
τ_β (ms)	0.45 ± 0.05	0.54 ± 0.04	0.48 ± 0.02
β (cm^{-1})	230 ● 19	211 ± 15	233 ± 9

ation of dopant ions in crystals,[43,51] glasses,[52] and polymers.[47] We carried out the fitting of the PA signal phase data of calcined and as-synthesized Cr-30 samples using eq 4. The nonradiative relaxation times, τ, and the optical absorption coefficients, β, of the 440- and 640-nm crystal field band of the Cr(III) in the as-synthesized sample and of the 370-nm charge-transfer band of Cr(VI) species in the calcined sample were measured using PA phase data fitting to the corresponding expression contribution for optically transparent and thermally thick samples. Figure 13 shows a typical result of data fitting for the phase data obtained at 440 nm, as a function of the modulation frequency ω. The results for each absorption band together with the obtained values of β and τ_β are summarized in Table V. Some conclusions might be drawn from the above results. First, the relaxation time, τ, is not expected for the level initially excited but rather for the average lifetime of a variety of states before energy is lost as heat. Thus, we may have a non-unique relaxation pathway consisting of several successive steps, and the measured lifetime is an average lifetime for heat production. Furthermore, for powdered samples, as is the case of the present work, τ also contains a contribution from the heat exchange time between the powder particles and the transducing gas of the PA cell. This heat exchange time depends not only on the shape of the particles but also on their size. The fact that the average of τ for Cr(III) in the as-synthesized sample is equal within the experimental error to the one obtained for the calcined sample shows that the mechanism of relaxation for Cr(VI) is not very different to the one used for Cr(III) to transfer the heat generated upon absorption of radiation.

(51) Murphy, J. C.; Aamordt, L. C. *J. Appl. Phys.* 1977, *48*, 3502.
(52) Lima, G. A. R.; Baesso, M. L.; Arguello, Z. P.; Silva, E. C.; Vargas, H.; Miranda, L. C. M. *Phys. Rev. B* 1987, *36*, 9812.

Conclusions

The combination of several physical techniques leads to the characterization of a chromium containing silicalite material prepared hydrothermally from a neutral fluoride suspension. The main conclusions are summarized below as follows:

PXRD-calculated unit cell volumes have shown that co-incorporation of small concentrations of chromium with aluminum, in a ZSM-5-type structure, still yields expanded unit cells.

The mid-IR spectra show a very week band around 680 cm^{-1}, whose intensity is not affected by ionic exchange or calcination, assigned to (Si–O–Cr) groups symmetrical stretching vibrations. Shoulders at the lower wavenumber side of the band around 1100 cm^{-1}, previously assigned to ν_a –(Si–O–M)$_n$–,[35] disappear after calcination and might be due to Si–OH or Si–F vibrations.[36]

EPR measurements have shown that there are two distorted Cr(III) species, A and B, in the chromium silicalite, none of which can be oxidized after 24 h, at 693 K under O_2 flow. One of them is ion exchanged in aqueous HCl solution. A third Cr(III) site, C, is spherically symmetric and is extensively oxidized to Cr(VI). This led us to propose that site A is the actual Si(IV) substitutional site in the silicalite framework, while site B is only a highly distorted channel-located Cr(III) species, probably cationic, whose nature is yet unknown. Site C contains charge-balancing and oxide-like Cr(III) species.

The optical absorption spectra measured by photoacoustic spectroscopy show the typical bands for Cr(III) at 440 nm ($^4A_2 \rightarrow {}^4T_1(F)$) and in 640 nm ($^4A_2 \rightarrow {}^4T_2$) and the charge-transfer band at 370 nm of Cr(VI) species and revealed the presence of unoxidized Cr(III) framework sites even after extensive oxidation.

By using special techniques and equipment, the photoacoustic spectroscopy allowed for the determination of the thermal diffusivity, α, of as-synthesized (0.041 ± 0.002 $cm^2\ s^{-1}$) and calcined (0.038 ± 0.002 $cm^2\ s^{-1}$) chromium silicalite samples, as well as their nonradiative relaxation times, τ and τ_β, and absorption coefficient for each band.

Acknowledgment. Financial support from FAPESP, CAPES, and CNPq is gratefully acknowledged. We are indebted to Prof. J. S. Barone for the chemical analysis.